Detection of miR-155 Using PNA at Physiological-Like Conditions by Surface Plasmon Resonance and bioFET

Francesco Lavecchia di Tocco , Valentina Botti , Salvatore Cannistraro , Anna Rita Bizzarri *

Posted Date: 26 December 2023

doi: 10.20944/preprints202312.1733.v1

Keywords: Biosensors; MicroRNA; Surface Plasmon Resonance; Field Effect Transistors

Article

Detection of miR-155 Using PNA at Physiological-like Conditions by Surface Plasmon Resonance and bioFET

Francesco Lavecchia di Tocco, Valentina Botti, Salvatore Cannistraro and Anna Rita Bizzarri *

Biophysics and Nanoscience Centre, DEB, Università della Tuscia, Largo dell'Università, 01100, Viterbo, Italy.
francesco.ditocco@unitus.it (FLT); valentina.botti@unitus.it (VB); cannistr@unitus.it (SC);
* Correspondence: bizzarri@unitus.it

Abstract: MicroRNAs are small ribonucleotides which act as key gene regulators. Their altered expression is often associated with onset and progression of several human diseases, including cancer. Given their potential use as biomarkers, there is a need to find detection methods of microRNAs suitable for use in clinical setting. Field Effect Transistor based biosensors (bioFETs) appear to be valid tools to detect microRNAs, since they may reliably quantitate the specific binding between the immobilized probe and free target in solution through an easily detectable electrical signal. We have investigated the detection of human microRNA 155 (miR-155) using an innovative capturing probe constituted by a synthetic peptide nucleic acid (PNA), which has the advantage to form a duplex even at ionic strengths approaching the physiological conditions. With the aim to develop an optimized BioFET setup, the interaction kinetics between miR-155 and the chosen PNA was preliminary investigated by Surface Plasmon Resonance (SPR). By exploiting both these results and our custom-made bioFET system, we were able to attain a low-cost, real-time, label-free, highly specific detection of miR-155 in the nano-molar range.

Keywords: biosensors; MicroRNA; surface plasmon resonance; field effect transistors

1. Introduction

MicroRNAs (miRNAs) are small non-coding nucleic acids of about 18-25 nucleotides which play a pivotal role in gene regulation of all superior organisms, including humans, and are involved in several cellular processes, such as proliferation, differentiation and apoptosis [1-3]. Given their physiological importance, deregulation of miRNAs is related to the development of numerous disease states, including multiple forms of cancer [4,5] Therefore, miRNAs are excellent molecular biomarkers with high potentialities in diagnostics [6-8]. However, their small size and low concentrations make the detection of miRNAs rather difficult. Currently, oligonucleotides are essentially detected by biomolecular techniques (e.g. real time PCR, northern blotting, microarray analysis) [9-11]. Although these methods may reach relatively high performances, their use in the clinical diagnostic field is rather hampered by several reasons. Indeed, they require long waiting times, necessitate the use of specific labels, and often involve extensive sample handling by highly specialized personnel with significant costs [12]. Biosensors technologies are susceptible to offer good solutions to the above-mentioned problems, allowing, additionally, optimized and sensitive clinical detection of miRNAs [13,14]. A biosensor is a device able to perceive biological events (e.g., the interaction between two molecular partners) and to transduce them in the form of a chemical, physical or electrical signal [15]. In the last decades, electrochemical biosensors, and in particular bio-Field Effect Transistor (bioFET) based device, have received great attention essentially because they can reach levels of sensitivity and specificity comparable to the canonical methods, being at the same time label-free, low cost, and presenting high potentiality to be automatized with no-or little sample pre-treatment [16-18]. Briefly, in a FET device, the electric current flows between two electrodes (source and drain) linked by a semiconductor channel; a third electrode (gate), coupled to the device

 doi:10.20944/preprints202312.1733.v1

through a thin dielectric layer, can modulate the conductance between the drain-source electrodes according to its voltage [19]. When specific biological probes, previously immobilized onto the gate surface, capture the target of interest a release of charges towards the gate electrode occurs. Accordingly, the change of the gate voltage will affect the source-drain current, allowing thus to correlate this variation to the target concentration [20]. However, current detection involves only the accumulated charges within the so-called Debye distance from the electrode which, in turn, strongly depends on the ionic strength of the solution [21,22]. Natural capturing probes for miRNAs are constituted by their complementary DNA or RNA strands which give rise to duplexes via a hybridization process. Since both partners display negatively charged phosphate backbones, a high ionic strength is required to optimize the hybridization process; about 500mM represents the optimum ionic strength to shield the electrostatic repulsion and to facilitate nucleic acid hybridization [23,24]. Therefore, such a constraint limits the bioFET capabilities: indeed, the greater the ionic strength of the working solution, the smaller is the Debye length within which the charges carried by the target miRNAs that can be perceived [21]. One promising solution to this problem may be represented by the use of peptide nucleic acids (PNAs) as capturing probe for miRNAs. PNAs are nucleotide analogues where the negative phosphate backbones are replaced by repeated units of N-(2- amminoetil)-glycine connected by peptide bond [25,26]. Accordingly, PNA, can hybridize with complementary nucleic acids at lower ionic strengths, when compared to canonical counterparts [27,28]; with a subsequent reduction of the Debye length leading to a substantial improvement of the bioFET detection capability. Therefore, this approach presents the important advantage to render accessible bioFET-based detection at physiological conditions which are usually characterized by an ionic strength of about 150mM [29]. However, the absence of the negative phosphate backbones also modifies the interaction kinetics between PNA and the complementary nucleic acids; and the relationship between ionic strength and PNA-miRNAs interaction on solid surfaces should be therefore investigated [30-33]. On such a basis, the present work has the objective of paving the way for the development of a bioFET-based biosensor for a clinically relevant microRNA at physiological-like conditions by using PNA molecules as capturing probes. Our target is microRNA 155 (miR-155), a multifunctional miRNA regulating B cell differentiation and development stages, by also playing a key role in the mammalian immune system [34,35]. MiR-155 is overexpressed in various malignant tumor cells, such as hepatocellular carcinoma, breast cancer, colon cancer [36,37] whose detection deserves high interest, as biomarker, in diagnostics and prognosis [38].

Since the kinetics can be strongly modulated by the ionic strength and, on the other hand, it could have a significant impact on the bioFET response, we have preliminary investigated the hybridization process between miR-155 and the related PNA by Surface Plasmon Resonance (SPR), to extract the association and dissociation rates under the experimental conditions of bioFET sensing [39,40]. We have then implemented a procedure on a custom-made bioFET setup to detect miR-155 at 150 mM ionic strength. The results indicate that our label-free, PNA-bioFET system is capable of a highly specific recognition of miR-155 with a limit of detection (LOD) in the nano-molar concentration under physiological-like conditions.

2. Materials and Methods

2.1. Materials

Single-stranded RNA oligonucleotides with the sequence of human miR-155-5p (5′-uaa ugc uaa ucg uga uag ggg-3′), the PNA complementary strands (5′-uag cuu auc aga cug aug uug a-3′, miR-21, 7.0 kDa), as well as miR-21-5p (5′-uag cuu auc aga cug aug uug a-3′, miR-21, 7.0 kDa), and miR-141-5p (5′-uaa cac ugu cug gua aag aug g-3′, miR-141, 7.1 kDa), were purchased from Metabion (Planegg, Germany) as dry pellets. The thiolated PNA oligomer with complementary sequence to miR-155 (5′-uag cuu auc aga cug aug uug a-3′, miR-21, 7.0 kDa) was synthesized by biomers.net (Ulm, Germany) and shipped in dry form as well. Oligos were purified by high-performance liquid chromatography−mass spectrometry (HPLC−MS). The pellets were resuspended in sterile 10mM sodium phosphate buffer (NaPi, 8.1 mM Na_2HPO_4, 1.9 mM NaH_2PO_4) in aliquots by 100μM

 doi:10.20944/preprints202312.1733.v1

concentration, miRs at pH= 7.8 and the PNA at pH=6, and then stored at 253 K. 6-mercapto-1-Hexanol (MCH) was purchased from Sigma-Aldrich Co. Work surface and equipment were decontaminated by using RNaseZap (Ambion; Sigma Aldrich Co.). Buffers were prepared using reagents from Sigma-Aldrich Co. and bi-distilled water; after having been microfiltered (Sartorius, Gottingen, Germany), they were stored at 277 K and thermalized at room temperature before experiments.

2.2. SPR Measurements

SPR experiments were conducted at 298 K with a Biacore X100 instrument (GE Healthcare, BioSciences AB, Uppsala, Sweden). The ligand PNA was immobilized onto a customizable Sensor Chip Au (GE Healthcare) surface, while the analyte miR-155 was fluxed free in solution over the ligand-functionalized sensorchip. Their interaction, upon leading to the analyte molecules to accumulate over the surface, produced changes in the refractive index of the medium, allowing then to monitor the process in real time through the induced shift in the SPR angle.

For the immobilization, thiolated PNA solutions were incubated for 1 h with 100 mM dithiothreitol (DTT) (Sigma-Aldrich Co.) in NaPi buffer at pH 8.0 in order to break the disulfide bond protecting the thiol (−SH) moiety; the obtained PNA-SH was eluted from NAP10 columns (GE Healthcare, USA) with working buffer (PBS, 6.84 mM Na2HPO4, 3.16 mM NaH2PO4, 126.32 mM NaCl, I = 150 mM, pH 7.2) for the removal of DTT. The sensorchip surface was cleaned with H^2O^2 (Merck Millipore, Darmstadt; Germany) under ultraviolet (UV) light for 30min, according to the so-called liquid-based hydrogen peroxide-mediated UV-photooxidation (liquid-UVPO) technique [Johnson et al.], washed with ultrapure water and dried with nitrogen. Once docked in the instrument, the chip was primed with running buffer (working buffer with 0.005% surfactant p20 (GE Healthcare). Using Manual Run (Biacore X100 software), an injection of 130 µL of a solution of 8 µM PNA-SH in working buffer at pH 7.2 was carried out exclusively in the measurement cell (Fc2) at a flow rate of 5 µL/min for 1080 s, while the control flow cell (Fc1) was not functionalized. Then, the Manual Run was immediately ended and the chip was kept docked in the instrument overnight, allowing incubation at 298 K. Afterwards, in order to passivate the Au surface, both flow cells were injected with 130 µL of a solution of 1 mM 6-mercapto-1-hexanol (MCH, Sigma- Aldrich Co.) in running buffer with 0.2% Ethanol (Sigma- Aldrich Co.), at a flow rate of 5 µL/min for 1080 s.

After a 5h incubation, unreacted groups were finally removed from the surface by the means of 30 s pulses of 100mM NaOH (Sigma- Aldrich Co.). In such a way, about 500 resonance units (RU) of PNA-SH were immobilized in Fc2; a rather low immobilization level was chosen to limit mass transport, rebinding and steric hindrance *[40].* Interaction analyses were performed by SCK and MCK kinetics assays. In SCK assays, five sequential increasing concentrations of miR-155 in running buffer (0.01, 10, 50, 175 and 750 nM) were injected over the PNA surface in both flow cells for 180 s, each followed by a 180 s dissociation step with running buffer; finally, each cycle was ended by a dissociation step of 1200s. In MCK assays, instead, in each cycle one of five increasingly higher concentrations (0.01−750 nM) of miR-155 was fluxed for 180 s, followed by a dissociation step of 1200 s with running buffer and by a 30 s pulse of regeneration solution (100mM NaOH) at 30 µL/min, used to unbind analyte molecules from the PNA on the surface. After preliminary tests, to prevent mass transport [40], the fastest flow rate (30 µL/min) that allowed to monitor the association step for the longest time was chosen. At the beginning of all assays, bare buffer flow was used to equilibrate the surface to provide the blank response which, in combination with the control response registered from Fc1, was used to correct the sensorgrams for non-specific binding to the surface, systematic noise, and instrumental drift. Experimental data was evaluated using the BiaEvaluation software 2.1 (GE Healthcare). Goodness of fits was estimated from the residual plots, χ^2 value, and U value, the latter estimating the uniqueness of the calculated parameters (not significantly correlated for $U < 15$) [41]. Measurements were conducted in triplicates.

2.3. Gold Sensing Area Functionalization

Screen-printed electrodes (DRP-220AT-U75, with gold sensing track area of 2.0 mm^2) were purchased from METROHM Italiana Srl. The gold sensing area of electrodes was cleaned and

 doi:10.20944/preprints202312.1733.v1

activated using the liquid-UVPO technique [42]. The biofunctionalization procedure of active electrodes by PNA exploited the formation of a self-assembled monolayer (SAM) through the thioester bond generated between the terminal thiol of PNA probes and the gold surface of electrodes [43]. It consisted of two steps separated by rinsing the gold surface with filtered (0.2 μm filtering membrane pore size) deionized water and drying by pure nitrogen. In the first step, the gold sensing area was incubated with 12 μL of a mixed solution of PBS (6.84 mM Na2HPO4, 3.16 mM NaH2PO4, 126.32 mM NaCl, I = 150 mM, pH 7.2) containing 350μM MCH and 15μM PNA for 3 hours at room temperature. The role of MCH molecules in the first co-immobilization step was to distance the PNA probes from each other, thus making them more accessible to binding with miR-155 [44-46]. In the second step, the electrodes were incubated with 12μL of PBS containing 1mM MCH for one hour at room temperature, to block the unreacted site of gold sensing area. For what concerns the control electrodes, only the second immobilization step was implemented maintained. The sensor surface of electrodes was then rinsed as described above and the sensors were used immediately.

2.4. BioFET Set Up and Electrical Measurements.

For electrical measurements, the functionalized electrodes were inserted into a printed circuit board (PCB) with integrated a commercial zero-threshold n-type metal oxide semiconductor field effect transistor (mosFET; ALD110900A from Advanced Linear Devices Inc., Sunnyvale, CA, USA). The electrodes were then horizontally inserted into a commercial fluidic cell (METROHM Italiana Srl) characterized by a conical opening able to accommodate the functionalized sensing area of electrode together with a commercial bulky Ag/AgCl reference electrode (DriRef-2, World Precision Instruments Ltd, Hitchin, UK). The use of the fluidic cell provides a high stability to the system. The conical opening of fluidic cell also allowed target injections to be performed in a controlled manner and in proximity to the functionalized electrode sensing area. The experimental measurements were carried out by a Keithley 2636B (TeKtronix, Beaverton; OR, USA), with a sensitivity in the fA range for current measurements and μV range for potential ones. Two source-mater units (SMUs) of the Keithley apparatus were used. The SMU1 applied the voltage (V_{ds}) between drain and source electrodes, which was kept constant at 100mV for all experiments, and measured the corresponding current flow (I_{ds}). The SMU2 applied a potential bias (V_{ref}) to reference electrode in solution. Biosensing experiments were carried out in NaPi 150mM pH=7.2 as working buffer (working volume of 200μL). The real-time assays were performed at constant V_{ds} (100mV) and V_{ref} (450mV) and the I_{ds} current was monitored over-time. 15μL volumes at increasing concentrations of miR-155 were added by pipetting into the conical opening of fluidic cell (the same working buffer was used to avoid current variation as result of change in pH or ionic strength in the solution *[47]*). The specificity tests were carried out in the same conditions described above but substituting mirR-155 with noncomplementary miRNAs. All biosensing experiments, as well as the control tests, were repeated three times.

3. Results and Discussion

3.1. SPR Investigation

The kinetics of PNA/miR-155 hybridization in physiological-like conditions has been investigated by SPR kinetic assays. Indeed, the SPR set up, although based on a continuous-flow microfluidic approach, allows to up-close mimic the conditions occurring in biosensing experiments, in which the molecular probe, immobilized on the gate surface, interacts with the target specimen free in solution. The gold-coated surfaces of the SPR sensor chips have been functionalized with PNA molecules (see Materials and Methods) and subsequently submitted to the flow of miR-155 in running buffer (NaPi, I=150mM, pH 7.2). Figure 1 shows the monitored response over time (sensorgram) of a representative single-cycle kinetic (SCK) assay, in which solutions of five increasing concentrations (0.01, 10, 50, 175, 750 nM) of miR-155 have been fluxed over a PNA-immobilized chip, separated by bare buffer injections of the same volume, and followed by a final, prolonged (1200s) flow of bare buffer.

Preprints (www.preprints.org) | NOT PEER-REVIEWED | Posted: 26 December 2023 doi:10.20944/preprints202312.1733.v1

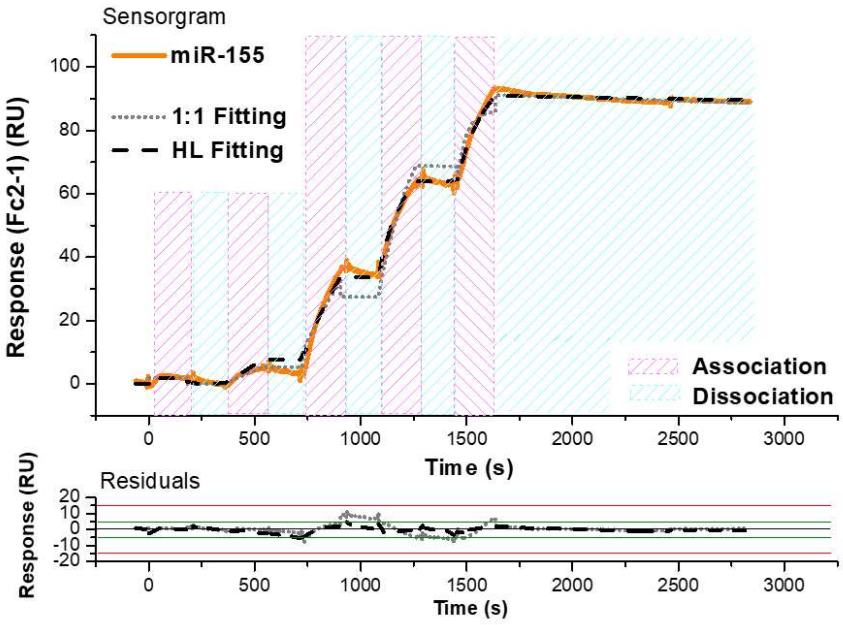

Figure 1. Top: SPR sensorgram (solid orange curve) of a representative SCK assay performed at 298 K upon injection of five increasing concentrations (0.01–750 nM) of miR-155 in running buffer over the PNA-functionalized sensor chip surface. Global fit of the sensorgram has been performed according to a 1:1 reversible bimolecular binding model (dotted grey curve; scoring $\chi^2 = 8.88$ RU^2) and to the Heterogeneous Ligand (HL) binding model (dashed black curve; scoring $\chi^2 = 2.54$ RU^2). Bottom: plot of the fitting residuals.

During miR-155 injections, the registered response presents a significant rise, signalling that more and more miR-155 molecules carried in the continuous flow of buffer are being held close to the surface, by specific interaction with PNA (association phase). Moreover, these ascending curves do not level out within the analyte injection period (180s), hinting to a rather slow dissociation rate. As the analyte carrying flow is substituted by buffer alone to promote removal of miR-155 from the surface (dissociation phase), a comparatively much smaller fall of the signal can be observed: the response decreases only by 5% on average, even after a long waiting time (1200s). These results indicate a quite strong and long-lived interaction between the partners. First, we have fitted the obtained sensorgram by the 1:1 Langmuir binding model, which assumes a simple reversible biomolecular reaction [48]. By obtaining a score of χ^2 =8.88, we found a value of (3.3±0.5) × 10^4 M^{-1} s^{-1} for the association rate constant (k_{on}) and of (2.4±0.3) × 10^{-5} s^{-1} for dissociation rate constant (k_{off}), leading to an equilibrium dissociation constant ($K_D = k_{off}/k_{on}$) of 0.7±0.5 nM. As shown in Figure 1, the 1:1 fitting curve shows slight deviations from the experimental data. Similar deviations from the Langmuir trend have been observed for the hybridization kinetics of oligonucleotides immobilized onto copolymer-coated glasses, and they have been ascribed to some inhomogeneity in the arrangement of molecules on the surface, giving rise to an accumulation of charges onto the surface and then to steric hindrance [49]. Accordingly, the sensorgrams have been analysed through the Heterogeneous Ligand (HL) binding model, which considers some heterogeneity in the layer of surface-attached molecules and describes the binding curve as the sum of two main independent sub-populations. HL fitting scores a better χ^2=2.54, with uniformly distributed residuals of small entity (see Figure 1), and identifies two equal-weight contributions characterized by: k_{on}^1= (1.2±0.6) × 10^4 M^{-1} $s^{-1}$and k_{off}^1=(1.2±0.2) × 10^{-5} s^{-1}, k_{on}^2=(2±1) × 10^5 M^{-1} s^{-1} and k_{off}^2=(4±2) × 10^{-5} s^{-1}; the corresponding equilibrium dissociation constant being K_D^1=1.1±0.6 nM and K_D^2=0.2±0.4 nM. Notably, the values of the association and dissociation rate constants extracted by the two applied models are quite similar; this suggesting that PNA/miR-155 hybridization can be suitably described by a 1:1 reversible reaction, while the heterogeneity in the PNA layer, possibly causing different accessibility to the surface binding sites, does not substantially alter the interaction kinetics. To further verify these

Preprints (www.preprints.org) | NOT PEER-REVIEWED | Posted: 26 December 2023 doi:10.20944/preprints202312.1733.v1

results, kinetic assays have been also performed by the multi-cycle kinetic (MCK) approach, in which a regeneration step is carried out after each miR-155 injection (see Materials and Methods). Since only minimum dissociation can be obtained by fluxing buffer alone, 30s long pulses of 100mM NaOH at 30µL/min have been used to remove from the surface miR-155 molecules hybridized to the PNA, before injecting the next concentration of miR-155. Such an approach, under the assumption that the repeated exposure to the regeneration solution does not alter the PNA layer, also allows to better estimate the value of k_{off}, as all the analyte injections are followed by prolonged (1200s) dissociation steps. In Figure 2, the sensorgrams of a representative MCK assay show progressively higher signals as the concentration of the injected miR-155 solutions increases from 0.01 to 750 nM.

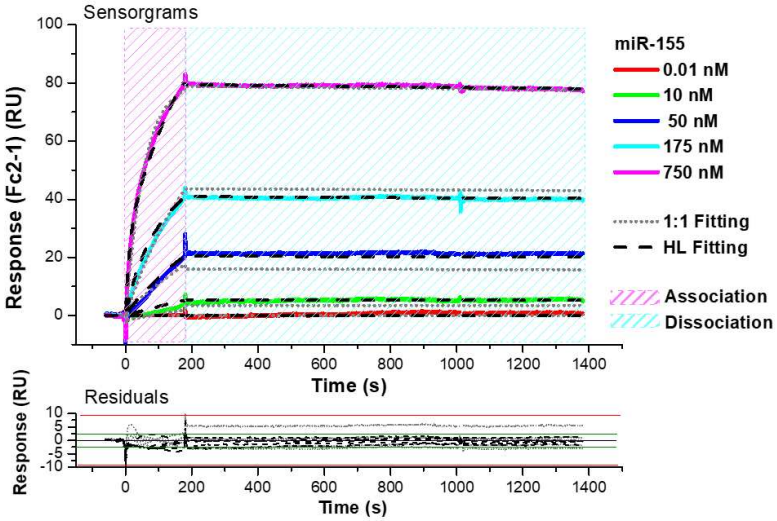

Figure 2. Top: SPR sensorgrams (solid-coloured curves) of the MCK assay performed at 298 K upon injection of five increasing concentrations (0.01−750 nM) of miR-155 in running buffer over the PNA-functionalized substrate. Global fit of the sensorgrams has been performed according to the 1:1 binding model (dotted grey curves; scoring χ^2 = 7.84 RU^2) and to the Heterogeneous Ligand (HL) binding model (dashed black curves; scoring χ^2 = 4.05 RU^2). Bottom: plot of the fitting residuals.

The trend of the sensorgrams is similar to that observed with the SCK approach, with response curves rising without reaching a plateau within the association phases and not significantly decreasing during the dissociation steps. A fitting of MCK data by the 1:1 Langmuir binding model, with χ^2=7.84, has provided: k_{on}= (2.3±0.6) × 10^4 M^{-1} s^{-1},k_{off}=(3±1) × 10^{-5} $s^{-1}$and K_D=1±1 nM. Conversely, the HL fitting, with χ^2=4.05, identifies two contributions: the main described by k_{on}^1= (2±1) × 10^4 M^{-1} s^{-1}, k_{off}^1=(2±1) × 10^{-5} s^{-1}, K_D^1=1±1 nM and the minor by k_{on}^2= (1±1) × 10^5 M^{-1} s^{-1}, k_{off}^2=(9±1) × 10^{-6} s^{-1}, K_D^2=0.1±0.1 nM. The MCK assay has provided association rates comparable to the ones obtained by the SCK method and even slower dissociation rates (at the detection limit), confirming a quite strong and long-lasting interaction between the partners. Accordingly, at the physiological ionic strength, the association between immobilized PNA and free miR-155 molecules is an efficient process, with hybridization occurring within rather short times. On the other hand, the complex dissociation rates are characterized by a very long lifetime, indicating that the formed duplex is quite stable. Notably, the found results indicate a more stable interaction in comparison to that observed between miR-155 and its complementary RNA strands (antimiR-155) in similar measurement conditions [50]. Finally, the resulting K_D values denote a high affinity which falls within the range observed for duplex formation of oligonucleotides free in solution [51]. To evaluate the specificity of the PNA-functionalized surface for the detection of miR-155, control SPR experiments with nontarget miRNAs have been performed. A sensor chip immobilized with PNA has been exposed to the flow of 1µM solutions in running buffer of miR-21; miR-141, miR-155 and a mix of all three miRNAs. For each case, the test has been repeated three times, with the surface being regenerated after each analyte injection. A comparison of all the collected SPR responses is shown in Figure 3.

Preprints (www.preprints.org) | NOT PEER-REVIEWED | Posted: 26 December 2023 doi:10.20944/preprints202312.1733.v1

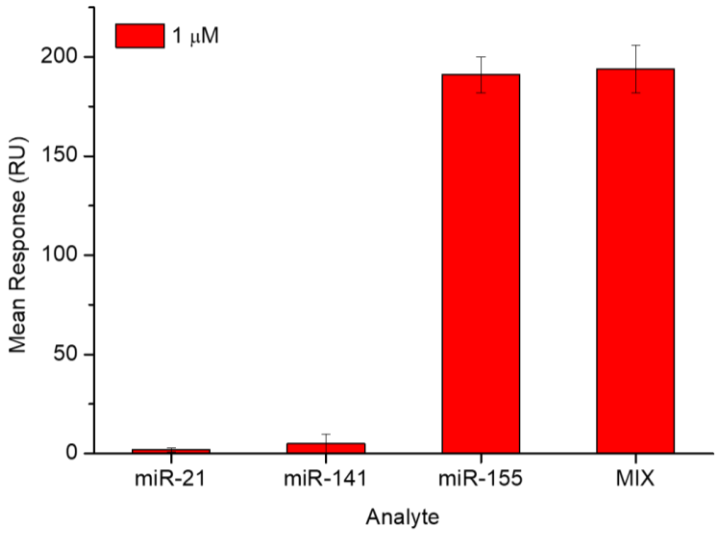

Figure 3. Comparison of SPR responses of a same PNA-functionalized sensor chip against the target (miR-155), two non-complementary miRNA strands (miR-141 and miR-21) and a mixture (MIX) of all three miRNAs, at the same concentration (1μM in running buffer).

A substantially negligible signal has been obtained for miR-21 and the response of miR-141 is 90% lower than that observed with miR-155, while the mix solution displays an intensity corresponding substantially to that of miR-155 alone. The used non-complementary miRNA strands did not generate a significant system's response; with this supporting the high specificity of the PNA towards miR-155.

3.2. Biosensing Analyses by a bioFET Setup

SPR results indicate that, in hundreds of seconds, the interaction between the partners has largely occurred. Although a direct extrapolation of the SPR results, which are obtained in microfluidic conditions, to bioFET experiments which are performed in static fluid conditions, cannot be done, this information may guide about the temporal window within which real time BioFET measurements can be reliably performed.

The gold sensing area of the electrodes (representing the functional extended gate of the bioFET system) has been functionalized with PNA molecules. In parallel, control electrodes without probes have been prepared (for more details see Materials and Methods). The gold electrodes have been subsequently connected to the gate of bioFET and inserted into the fluidic cell, which was, in turn, filled with a working buffer solution identical to that used for SPR assays. In all experiments, prior to real biosensing analyses, the real-time current has been registered until it reached a plateau sufficient to ease later biosensing tests and the related signal evaluation [52]. In this regard, it has been decided to start of the injections an average current variation of less than 0.01uA over 200s. Notably, electrodes have reached the stability in slightly different times; with this being likely due to small fabrication differences between electrodes and to the heterogeneity of the functionalized layers. However, in almost all the cases the stability has been reached within a waiting time from 1000 to 2000 s. After current stabilization, multiple injections of solutions containing increasing concentrations of miR-155 have been performed, at 100 s time intervals, on both active and control electrodes by continuously recording the current.

Figure 4A,B show the real-time responses of representative biosensing assays performed on both the active and control electrodes, respectively, by adding successive solutions of miR-155 at 10, 50, 100, 150 nM concentrations.

Upon adding a miR-155 containing solution, a rapid current drop occurs, followed by a rise which reaches a sort of equilibrium, indicating that the hybridization of miR-155 molecules with

Preprints (www.preprints.org) | NOT PEER-REVIEWED | Posted: 26 December 2023 doi:10.20944/preprints202312.1733.v1

PNA probes has occurred. Such a behaviour finds a correspondence with the SPR results and indicates that immobilized PNA probes efficiently capture the target miR-155 in solution, within a relatively short time (about 100s).

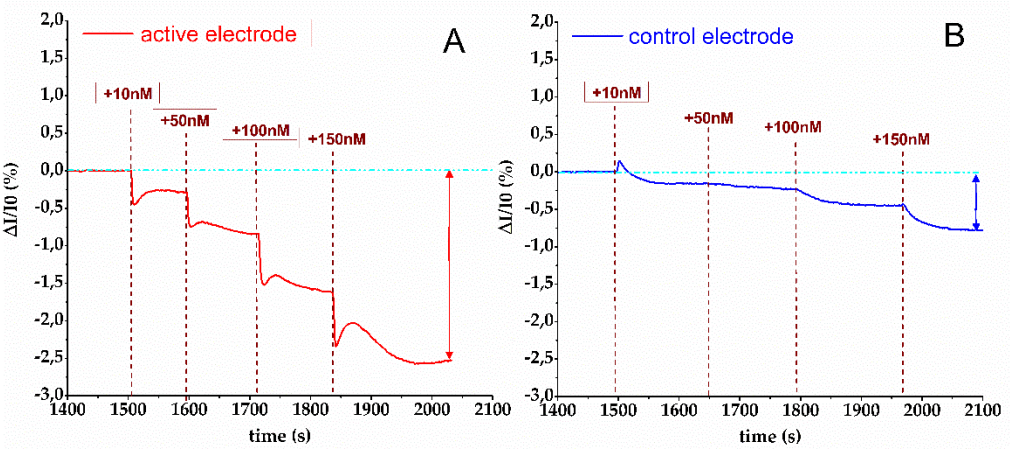

Figure 4. Real time biosensing analysis. Sequential injections of miR-155 at increasing concentrations (10nM, 50nM, 100nM and 200nM) on PNA-functionalized active electrode (A) and on MCH control electrode (B). .

To compare the injection effects occurred on different electrodes, the current value after stabilization has been normalized to the current variation according to the formula $(I_{ds}-I_0)/I_0 = \Delta I/I_0$, where I_{ds} stands for the real-time recorded current while I_0 is the current value obtained just after stabilization [53]. As shown in Figure 4A, drops of I_{ds} are detected in all the cases, upon adding solutions containing the target. Such a behaviour is consistent with the negative charges that are released to the gate by the captured miR-155 molecules at pH=7.2 [52] and with the fact that our bioFET uses a n-type transistor in which the main electric carriers are electrons. Indeed, in these operative conditions, the negative charges provided by the miR-155 molecules move away the electrons from the conductive channel, connecting the drain and source electrodes, and cause a decrease in the recoded I_{ds}. Furthermore, progressively higher current drops are detected as far as the concentration of the target in the fluidic cell increases.

Injections of miR-155 carried out on the control electrode (see Figure 4B) have yielded a much lower decrease in current. These I_{ds} variations could be attributed to random non-specific adsorption which may persist even after passivation of the gold electrode surface [54]. With the aim of eliminating contributions given by such non-specific interactions we have subtracted from the current variations of the active electrodes the corresponding current detected for the control electrodes ($\Delta I/I_{0(A)} - \Delta I/I_{0(C)}$).

Notably, the very long dissociation time evaluated by SPR allows us to approximate that the almost totality of the PNA-bound miR-155 molecules will not have dissociated by the end of the measurement (i.e. within 600 s after the first injection); and indeed,

Notably, the final I_{ds} response corresponds to the total miR-155 concentration (as obtained by cumulating the different injections) [55]. Accordingly, the effective concentrations of miR-155 in the fluidic cell at each step are about 10, 60, 160 and 310 nM. The obtained signal variations have been plotted *vs.* the miR-155 concentration to construct the calibration plot, as shown in Figure 5.

Preprints (www.preprints.org) | NOT PEER-REVIEWED | Posted: 26 December 2023 doi:10.20944/preprints202312.1733.v1

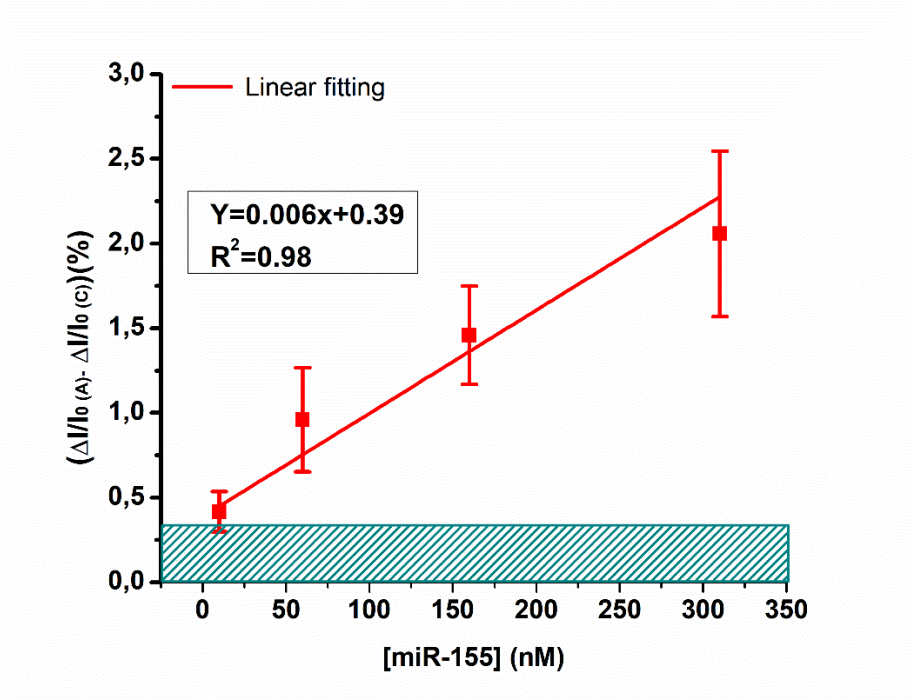

Figure 5. BioFEF calibration curve obtained by plotting the normalized current variation vs. miR-155 concentration. Red squares indicate the current variation observed by injecting miR-155 on active PNA electrode $\Delta I/I_{0(A)}$ minus the variations associated to same injections on control electrodes ($\Delta I/I_{0(C)}$). The barred box at the bottom represents the signal associated with buffer injections plus 3 times the relative standard deviation. .

The PNA-bioFET system response is characterized by a good linearity as witnessed by the R^2 = 0.988 value. Globally, these results indicate that bioFET allows a robust and sensitive detection of miR-155 at 150mM ionic strength, in agreement with kinetic characteristics found in SPR (fast association, slow dissociation and high affinity interaction).

Furthermore, single injections of working buffer have been performed on active electrodes with the aim to obtain the blank signal required for the calculation of the limit of detection (LOD) of our system; such a quantity being defined by IUPAC as the smallest measure that can be reasonably detected for a given analytical procedure, and which is obtained by the blank signal incremented by a certain number of times [56]. Here, the LOD has been calculated as the average signal obtained by blank injections plus three times relative standard deviation (barred box at the bottom of figure 5) [53,57]. Following this criterion, we have found a LOD of about 5nM. Such a value is similar to that found in other bioFET setups for small single strand DNA [58,59] and in other electrochemical biosensors for microRNAs detection [60,61].

Finally, the specificity of the bioFET setup has been evaluated by adding the same non-complementary miRNAs (miR-21 and miR-141) as done in SPR testing. For this purpose, sequential injections of miR-21, miR-141 and miR-155 at concentration of 150nM have been carried out on the active electrodes. The collected PNA-bioFET responses are shown in Figure 6.

Preprints (www.preprints.org) | NOT PEER-REVIEWED | Posted: 26 December 2023 doi:10.20944/preprints202312.1733.v1

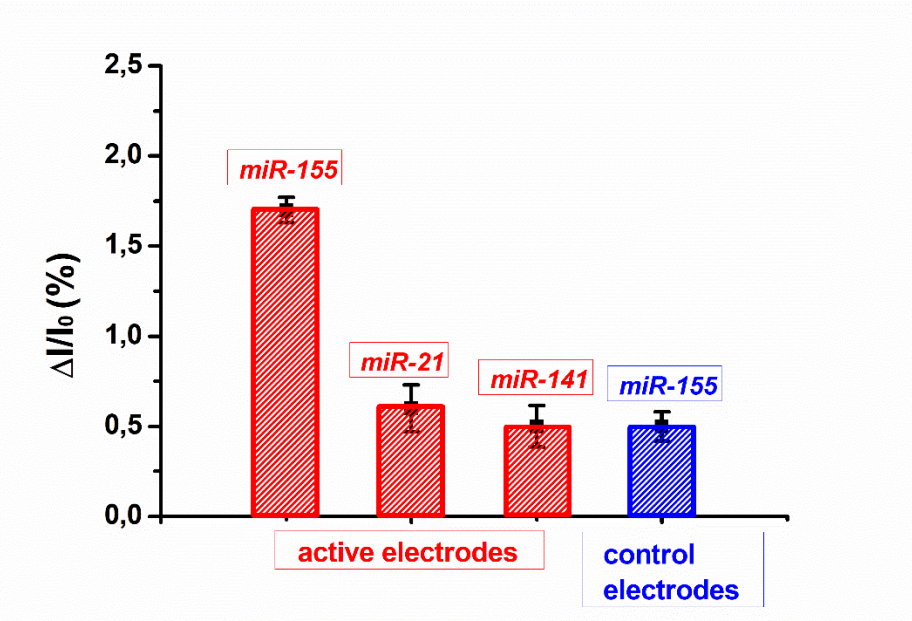

Figure 6. Normalized current variation associated to miR-155, miR-21 and miR-141 injections on active electrodes (red) and associated to miR-155 injections on control electrode (blue).

Non-complementary miRNA injections have yielded a much lower current variation, which is indeed comparable to that occurring when miR-155 is injected to non PNA-functionalized electrodes (control electrodes in Fig 6, blue box). The residual activity for nonspecific miRNAs could be explained in terms of non-specific adsorption; in some respect being favoured by the static nature of electrode wetting in our bioFET system [54].

4. Conclusions

PNA molecules revealed to be extremely promising capture probes for miR-155 allowing to reach an efficient hybridization even at relatively low ionic strengths. The investigation by SPR of the interaction kinetics between PNA molecules immobilized on a gold-coated surface with miR-155 in fluxed solution at an ionic strength of 150 mM, has provided an association and dissociation rates of k_{on}= 2 ·10^4 M^{-1} s^{-1} and k_{off}=2 · 10^{-5} s^{-1}, respectively, and an affinity of about 10^9 M^{-1}. These results, on one hand, indicate that PNA can hybridize miR-155 even at the ionic strengths mimicking the physiological conditions, and, on the other, that they may represent a optimal capture probe for bioFET experiments. BioFET measurements performed by successive injections at progressively higher concentrations of miR-155 have allowed us to extract a biosensing calibration plot characterized by a very good linearity in the 10-150 nM miR-155 concentration range and showing a LOD of about 5 nM. Control bioFET experiments with other miRNAs, such as miR-21 and miR-141, have shown that PNA is quite specific in capturing miR-155. The remarkable performance reached in the present study in terms of rapidity, specificity, absence of labels indicates that our bioFET sensing approach could be very promising to be translated in clinical diagnostics in physiological fluids.

Author Contributions: Conceptualization, ARB and SC; Methodology, FDT,VB and ARB.; measurements, FDT.,VB.; software and experimental analysis, FDT,VB and ARB writing original draft—review and editing, FDT,VB, SC and ARB All authors have read and agreed to the published version of the manuscript.

Funding: This research was funded by Italian Association for Cancer Research (AIRC) (Grant IG24450 to ARB).

Institutional Review Board Statement: Not applicable.

Informed Consent Statement: Not applicable.

Data Availability Statement: Not applicable.

References

1. Bartel DP. MicroRNAs: genomics, biogenesis, mechanism, and function. Cell. 2004 Jan 23;116(2):281-97. doi: 10.1016/s0092-8674(04)00045-5. PMID: 14744438.
2. Ambros V. The functions of animal microRNAs. Nature. 2004 Sep 16;431(7006):350-5. doi: 10.1038/nature02871. PMID: 15372042.
3. Hammond SM. An overview of microRNAs. Adv Drug Deliv Rev. 2015 Jun 29;87:3-14. doi: 10.1016/j.addr.2015.05.001. Epub 2015 May 12. PMID: 25979468; PMCID: PMC4504744.
4. Macfarlane LA, Murphy PR. MicroRNA: Biogenesis, Function and Role in Cancer. Curr Genomics. 2010 Nov;11(7):537-61. doi: 10.2174/138920210793175895. PMID: 21532838; PMCID: PMC3048316.
5. Vaghf A, Khansarinejad B, Ghaznavi-Rad E, Mondanizadeh M. The role of microRNAs in diseases and related signaling pathways. Mol Biol Rep. 2022 Jul;49(7):6789-6801. doi: 10.1007/s11033-021-06725-y. Epub 2021 Oct 31. PMID: 34718938.
6. Bertoli G, Cava C, Castiglioni I. MicroRNAs: New Biomarkers for Diagnosis, Prognosis, Therapy Prediction and Therapeutic Tools for Breast Cancer. Theranostics. 2015 Jul 13;5(10):1122-43. doi: 10.7150/thno.11543.
7. Edwards JK, Pasqualini R, Arap W, Calin GA. MicroRNAs and ultraconserved genes as diagnostic markers and therapeutic targets in cancer and cardiovascular diseases. J Cardiovasc Transl Res. 2010 Jun;3(3):271-9. doi: 10.1007/s12265-010-9179-5. Epub 2010 May 5.
8. Basak I, Patil KS, Alves G, Larsen JP, Møller SG. microRNAs as neuroregulators, biomarkers and therapeutic agents in neurodegenerative diseases. Cell Mol Life Sci. 2016 Feb;73(4):811-27. doi: 10.1007/s00018-015-2093-x. Epub 2015 Nov 25. PMID: 26608596.
9. Li W, Ruan K. MicroRNA detection by microarray. Anal Bioanal Chem. 2009 Jun;394(4):1117-24. doi: 10.1007/s00216-008-2570-2. Epub 2009 Jan 9.
10. Válóczi A, Hornyik C, Varga N, Burgyán J, Kauppinen S, Havelda Z. Sensitive and specific detection of microRNAs by northern blot analysis using LNA-modified oligonucleotide probes. Nucleic Acids Res. 2004 Dec 14;32(22):e175. doi: 10.1093/nar/gnh171.
11. Hu Y, Lan W, Miller D. Next-Generation Sequencing for MicroRNA Expression Profile. Methods Mol Biol. 2017;1617:169-177. doi: 10.1007/978-1-4939-7046-9_
12. Zhu CS, Zhu L, Tan DA, Qiu XY, Liu CY, Xie SS, Zhu LY. Avenues Toward microRNA Detection In Vitro: A Review of Technical Advances and Challenges. Comput Struct Biotechnol J. 2019 Jun 20;17:904-916. doi: 10.1016/j.csbj.2019.06.018.
13. Johnson BN, Mutharasan R. Biosensor-based microRNA detection: techniques, design, performance, and challenges. Analyst. 2014 Apr 7;139(7):1576-88. doi: 10.1039/c3an01677c.
14. Turner AP. Biosensors: sense and sensibility. Chem Soc Rev. 2013 Apr 21;42(8):3184-96. doi: 10.1039/c3cs35528d. Epub 2013 Feb 19.
15. Bhalla N, Jolly P, Formisano N, Estrela P. Introduction to biosensors. Essays Biochem. 2016 Jun 30;60(1):1-8. doi: 10.1042/EBC20150001.
16. Cardoso AR, Moreira FTC, Fernandes R, Sales MGF. Novel and simple electrochemical biosensor monitoring attomolar levels of miRNA-155 in breast cancer. Biosens Bioelectron. 2016 Jun 15;80:621-630. doi: 10.1016/j.bios.2016.02.035. Epub 2016 Feb 14.
17. Mansouri Majd S, Salimi A, Astinchap B. Label-free attomolar detection of lactate based on radio frequency sputtered of nickel oxide thin film field effect transistor. Biosens Bioelectron. 2017 Jun 15;92:733-740. doi: 10.1016/j.bios.2016.09.097. Epub 2016 Sep 28.
18. Gutiérrez-Sanz, Ó.; Andoy, N.M.; Filipiak, M.S.; Haustein, N.; Tarasov, A. Direct, Label-Free, and Rapid Transistor-Based Immunodetection in Whole Serum. ACS Sensors 2017, 2, 1278–1286, doi:10.1021/acssensors.7b00187.
19. Lowe BM, Sun K, Zeimpekis I, Skylaris CK, Green NG. Field-effect sensors - from pH sensing to biosensing: sensitivity enhancement using streptavidin-biotin as a model system. Analyst. 2017 Nov 6;142(22):4173-4200. doi: 10.1039/c7an00455a.
20. Sung D, Koo J. A review of BioFET's basic principles and materials for biomedical applications. Biomed Eng Lett. 2021 Apr 9;11(2):85-96. doi: 10.1007/s13534-021-00187-8.
21. Tadmor, R., Hernández-Zapata, E., Chen, N., Pincus, P., & Israelachvili, J. N. (2002). Debye length and double-layer forces in polyelectrolyte solutions. Macromolecules, 35(6), 2380-2388.
22. Schasfoort, R. B., Bergveld, P., Kooyman, R. P. H., & Greve, J. (1990). Possibilities and limitations of direct detection of protein charges by means of an immunological field-effect transistor. Analytica chimica acta, 238, 323-329.
23. Gong P, Levicky R. DNA surface hybridization regimes. Proc Natl Acad Sci U S A. 2008 Apr 8;105(14):5301-6. doi: 10.1073/pnas.0709416105. Epub 2008 Apr 1..
24. Shakeel, Shabih, Sajjad Karim, and Arif Ali. "Peptide nucleic acid (PNA)—a review." Journal of Chemical Technology & Biotechnology: International Research in Process, Environmental & Clean Technology 81.6 (2006): 892-899.

25. Saarbach J, Sabale PM, Winssinger N. Peptide nucleic acid (PNA) and its applications in chemical biology, diagnostics, and therapeutics. Curr Opin Chem Biol. 2019 Oct;52:112-124. doi: 10.1016/j.cbpa.2019.06.006. Epub 2019 Sep 18.
26. Ananthanawat C, Vilaivan T, Hoven VP, Su X. Comparison of DNA, aminoethylglycyl PNA and pyrrolidinyl PNA as probes for detection of DNA hybridization using surface plasmon resonance technique. Biosens Bioelectron. 2010 Jan 15;25(5):1064-9. doi: 10.1016/j.bios.2009.09.028. Epub 2009 Oct 1.
27. Schwarz FP, Robinson S, Butler JM. Thermodynamic comparison of PNA/DNA and DNA/DNA hybridization reactions at ambient temperature. Nucleic Acids Res. 1999 Dec 15;27(24):4792-800. doi: 10.1093/nar/27.24.4792.
28. Nakatsuka N, Yang KA, Abendroth JM, Cheung KM, Xu X, Yang H, Zhao C, Zhu B, Rim YS, Yang Y, Weiss PS, Stojanović MN, Andrews AM. Aptamer-field-effect transistors overcome Debye length limitations for small-molecule sensing. Science. 2018 Oct 19;362(6412):319-324. doi: 10.1126/science.aao6750. Epub 2018 Sep 6.
29. Park H, Germini A, Sforza S, Corradini R, Marchelli R, Knoll W. Effect of ionic strength on PNA-DNA hybridization on surfaces and in solution. Biointerphases. 2007 Jun;2(2):80-8. doi: 10.1116/1.2746871.
30. Irving D, Gong P, Levicky R. DNA surface hybridization: comparison of theory and experiment. J Phys Chem B. 2010 Jun 10;114(22):7631-40. doi: 10.1021/jp100860z.
31. Kaisti M, Kerko A, Aarikka E, Saviranta P, Boeva Z, Soukka T, Lehmusvuori A. Real-time wash-free detection of unlabeled PNA-DNA hybridization using discrete FET sensor. Sci Rep. 2017 Nov 16;7(1):15734. doi: 10.1038/s41598-017-16028-7.
32. Papamatthaiou S, Estrela P, Moschou D. Printable graphene BioFETs for DNA quantification in Lab-on-PCB microsystems. Sci Rep. 2021 May 10;11(1):9815. doi: 10.1038/s41598-021-89367-1.
33. Faraoni I, Antonetti FR, Cardone J, Bonmassar E. miR-155 gene: a typical multifunctional microRNA. Biochim Biophys Acta. 2009 Jun;1792(6):497-505. doi: 10.1016/j.bbadis.2009.02.013. Epub 2009 Mar 5.
34. Due H, Svendsen P, Bødker JS, Schmitz A, Bøgsted M, Johnsen HE, El-Galaly TC, Roug AS, Dybkær K. miR-155 as a Biomarker in B-Cell Malignancies. Biomed Res Int. 2016;2016:9513037. doi: 10.1155/2016/9513037. Epub 2016 May 16.
35. Zhang Y, Li M, Wang H, Fisher WE, Lin PH, Yao Q, Chen C. Profiling of 95 microRNAs in pancreatic cancer cell lines and surgical specimens by real-time PCR analysis. World J Surg. 2009 Apr;33(4):698-709. doi: 10.1007/s00268-008-9833-0.
36. Mattiske S, Suetani RJ, Neilsen PM, Callen DF. The oncogenic role of miR-155 in breast cancer. Cancer Epidemiol Biomarkers Prev. 2012 Aug;21(8):1236-43. doi: 10.1158/1055-9965.EPI-12-0173. Epub 2012 Jun 26.
37. Hou Y, Wang J, Wang X, Shi S, Wang W, Chen Z. Appraising MicroRNA-155 as a Noninvasive Diagnostic Biomarker for Cancer Detection: A Meta-Analysis. Medicine (Baltimore). 2016 Jan;95(2):e2450. doi: 10.1097/MD.0000000000002450.
38. Moscetti I, Cannistraro S, Bizzarri AR. Surface Plasmon Resonance Sensing of Biorecognition Interactions within the Tumor Suppressor p53 Network. Sensors (Basel). 2017 Nov 20;17(11):2680. doi: 10.3390/s17112680.
39. Nguyen, H. H.; Park, J.; Kang, S.; Kim, M. Surface Plasmon Resonance: A Versatile Technique for Biosensor Applications. Sensors. 2015, pp 10481–10510.
40. Marquart, J. A. Surface Plasmon Resonance and Biomolecular Interaction Analysis-Theory and Practice; Pumbo BV, 2013. www.sprpages.nl.
41. GE Healthcare. Biacore Assay Handbook; General Electric Company, 2012.
42. Blake N. Johnson and Raj MutharasanThe Journal of Physical Chemistry C 2013 117 (3), 1335-1341DOI: 10.1021/jp307983e
43. Meng X, O'Hare D, Ladame S. Surface immobilization strategies for the development of electrochemical nucleic acid sensors. Biosens Bioelectron. 2023 Oct 1;237:115440. doi: 10.1016/j.bios.2023.115440. Epub 2023 Jun 16.
44. Rastislav Levicky, Tonya M. Herne, Michael J. Tarlov, and Sushil K. Satija Journal of the American Chemical Society 1998 120 (38), 9787-9792 DOI: 10.1021/ja981897r
45. Movilli J, Rozzi A, Ricciardi R, Corradini R, Huskens J. Control of Probe Density at DNA Biosensor Surfaces Using Poly(l-lysine) with Appended Reactive Groups. Bioconjug Chem. 2018 Dec 19;29(12):4110-4118. doi: 10.1021/acs.bioconjchem.8b00733. Epub 2018 Nov 26.
46. Mateo-Martí E, Briones C, Román E, Briand E, Pradier CM, Martín-Gago JA. Self-assembled monolayers of peptide nucleic acids on gold surfaces: a spectroscopic study. Langmuir. 2005 Oct 11;21(21):9510-7. doi: 10.1021/la050366v.
47. Chen S., Nyholm L., Jokilaakso N., Karlstrm A.E., Linnros J., Smith U., Zhang S.L. Current instability for silicon nanowire field-effect sensors operating in electrolyte with platinum gate electrodes. Electrochem. Solid-State Lett. 2011;14 doi: 10.1149/1.3584082.
48. O'Shannessy DJ, Brigham-Burke M, Soneson KK, Hensley P, Brooks I. Determination of rate and equilibrium binding constants for macromolecular interactions using surface plasmon resonance: use of

nonlinear least squares analysis methods. Anal Biochem. 1993 Aug 1;212(2):457-68. doi: 10.1006/abio.1993.1355.
49. Vanjur L, Carzaniga T, Casiraghi L, Chiari M, Zanchetta G, Buscaglia M. Non-Langmuir Kinetics of DNA Surface Hybridization. Biophys J. 2020 Sep 1;119(5):989-1001. doi: 10.1016/j.bpj.2020.07.016. Epub 2020 Jul 29.
50. Botti V, Lavecchia di Tocco F, Cannistraro S, Bizzarri AR. Hybridization Kinetics of miR-155 on Gold Surfaces as Investigated by Surface Plasmon Resonance and Atomic Force Spectroscopy. ACS Omega. 2023 Oct 9;8(42):38941-38949. doi: 10.1021/acsomega.3c03318.
51. Jing Z, Qi R, Thibonnier M, Ren P. Molecular Dynamics Study of the Hybridization between RNA and Modified Oligonucleotides. J Chem Theory Comput. 2019 Nov 12;15(11):6422-6432. doi: 10.1021/acs.jctc.9b00519. Epub 2019 Oct 9.
52. Zhang J, Lang HP, Yoshikawa G, Gerber C. Optimization of DNA hybridization efficiency by pH-driven nanomechanical bending. Langmuir. 2012 Apr 17;28(15):6494-501. doi: 10.1021/la205066h. Epub 2012 Apr 2.
53. Wang X, Dai C, Wu Y, Liu Y, Wei D. Molecular-electromechanical system for unamplified detection of trace analytes in biofluids. Nat Protoc. 2023 Jul;18(7):2313-2348. doi: 10.1038/s41596-023-00830-x. Epub 2023 May 19.
54. Cai B, Wang S, Huang L, Ning Y, Zhang Z, Zhang GJ. Ultrasensitive label-free detection of PNA-DNA hybridization by reduced graphene oxide field-effect transistor biosensor. ACS Nano. 2014 Mar 25;8(3):2632-8. doi: 10.1021/nn4063424. Epub 2014 Feb 20.
55. Chen Y, Ren R, Pu H, Guo X, Chang J, Zhou G, Mao S, Kron M, Chen J. Field-Effect Transistor Biosensor for Rapid Detection of Ebola Antigen. Sci Rep. 2017 Sep 8;7(1):10974. doi: 10.1038/s41598-017-11387-7.
56. Jenkins, R., Manne, R., Robin, R., & Senemaud, C. (1991). IUPAC—nomenclature system for x-ray spectroscopy. X-Ray Spectrometry, 20(3), 149-155.
57. Minamiki T., Sasaki Y., Tokito S., Minami T. Label-free direct electrical detection of a histidine-rich protein with sub-femtomolar sensitivity using an organic field-effect transistor. ChemistryOpen. 2017;6:472–475
58. Kaisti M, Kerko A, Aarikka E, Saviranta P, Boeva Z, Soukka T, Lehmusvuori A. Real-time wash-free detection of unlabeled PNA-DNA hybridization using discrete FET sensor. Sci Rep. 2017 Nov 16;7(1):15734. doi: 10.1038/s41598-017-16028-7.
59. Papamatthaiou, Sotirios, Pedro Estrela, and Despina Moschou. "Printable graphene BioFETs for DNA quantification in Lab-on-PCB microsystems." Scientific Reports 11.1 (2021): 9815.
60. Moccia M, Caratelli V, Cinti S, Pede B, Avitabile C, Saviano M, Imbriani AL, Moscone D, Arduini F. Paper-based electrochemical peptide nucleic acid (PNA) biosensor for detection of miRNA-492: a pancreatic ductal adenocarcinoma biomarker. Biosens Bioelectron. 2020 Oct 1;165:112371. doi: 10.1016/j.bios.2020.112371. Epub 2020 Jun 8.
61. Roychoudhury A, Dear JW, Bachmann TT. Proximity sensitive detection of microRNAs using electrochemical impedance spectroscopy biosensors. Biosens Bioelectron. 2022 Sep 15;212:114404. doi: 10.1016/j.bios.2022.114404. Epub 2022 May 20.